Collapse of the superradiant phase and multiple quantum phase transitions for Bose-Einstein condensates in an optomechanical cavity

Zhimei Wang,[1] Jinling Lian,[2] J.-Q. Liang,[1,*] Yanmei Yu,[3,†] and Wu-Ming Liu[3,‡]

[1]*Institute of Theoretical Physics and Department of Physics, Shanxi University, Taiyuan 030006, China*

[2]*Department of Physics, Shaoxing University, Shaoxing 312000, China*

[3]*Beijing National Laboratory for Condensed Matter Physics, Institute of Physics, Chinese Academy of Sciences, Beijing 100190, China*

(Received 10 August 2015; revised manuscript received 19 January 2016; published 15 March 2016)

We investigate the multiple stable macroscopic quantum states of a Bose-Einstein condensate in an optomechanical cavity with pump-cavity field detuning and atom-photon interaction following the experimental realization of the quantum phase transition [Nature (London) **464**, 1301 (2010)]. The spin-coherent-state variational method is useful in exploring the multistability since it has the advantage of including both normal and inverted pseudospin states. In the blue detuning regime the usual transition from normal to superradiant phases still exists, however, when the atom-field coupling increases to a certain value, called the turning point, the superradiant phase collapses due to the resonant damping of the mechanical oscillator. As a consequence, the system undergoes at this point an additional phase transition to the normal phase of the atomic population inversion state. In particular, the superradiant phase disappears completely at strong photon-phonon interaction, resulting in the direct atomic population transfer between two atomic levels. Moreover, the coupling-induced collapse and revival of the superradiant state are also found in the red detuning region.

DOI: 10.1103/PhysRevA.93.033630

I. INTRODUCTION

The realization of a Bose-Einstein condensate (BEC) in a dilute atomic gas [1,2] opened a new avenue of research in quantum many-body physics with the unique opportunity to simulate quantum optical and condensed matter phenomena [3,4]. Theoretical investigations have extended to BECs in the optical cavity [5] and the optical lattice [6–8] with spin-orbit coupling as well [9,10]. An ultracold atomic ensemble interacting with high-finesse cavity modes is a typical system of cavity quantum electrodynamics, which has witnessed significant development [11,12] in both quantum optics and cold-atom physics. Theoretically, the collective phenomenon in the light-matter system [13,14] was investigated long ago with the well-known Dicke model [15]. The fascinating quantum phase transition (QPT) from a normal phase to the superradiant phase has attracted particular interest in recent years, since it has a wide range of applications [16]. The existence of the coherent superradiant state at zero temperature [17] is considered an intriguing many-body phenomenon resulting from the collective effects. The experimental observation [13,18–21] of the QPT being a milestone in the cavity BEC has triggered active studies including experiments in an open cavity [22,23], which leads to theoretical explanations of the nonequilibrium QPT [24–27].

On the other hand, with a cavity mode being strongly coupled to a high-quality mechanical oscillator through radiation pressure [28–33], a new frontier known as cavity optomechanics [28,29] has been achieved with the recent technical progress [34–39] in exploring the coherent coupling between electromagnetic and mechanical degrees of freedom [40] in the quantum domain [41–50]. The optomechanical cavity provides many interesting phenomena such as optical cooling [36,51–54], optical bistability [55] in the optical domain, confinement [56–58] of the element, optical nonlinearity [55,59], and squeezing [41,50]. The cavity optomechanical sensor has also been developed in the strong-coupling [48] and quantum-coherent coupling [60] regimes.

The QPT in the Dicke model through mechanical vibrations [61] has been explored theoretically and the multistability of the BEC was found in the optomechanical cavity [62]. The measurement of the photon number [63,64] in a Fabry-Pérot cavity [65,66] provides a possibility to observe the QPT, which is no doubt of conceptual and technical importance for the BEC in an optomechanical cavity. Recently, the ground-state property of a BEC in an optomechanical cavity was investigated theoretically [67] by means of the Holstein-Primakoff transformation in the thermodynamic limit ($N \to \infty$). Since the nonlinear atom-photon interaction [23,68] is required in the actual experiment to realize the QPT, in the present paper we study theoretically the QPT with this interaction for a BEC in the optomechanical cavity. The variation of the nonlinear interaction in a wide range along with the pump-cavity field detuning can change the effective frequency of the cavity mode from positive to negative values. Thus, multiple stable states become possible [69]. It is certainly of interest to explore the effect of the mechanical oscillator on the multistability and related QPT.

The spin-coherent-state (SCS) variational method has the advantage of including both the normal $\Downarrow$ and inverted $\Uparrow$ pseudospin states, which are necessary for multistability. The inverted pseudospin state was first demonstrated in a dynamic study to reveal the multiple steady states in the nonequilibrium [24–27] QPT. Indeed, the inverted pseudospin $\Uparrow$ leads to the stable state of atomic population inversion and the inverted QPT in the presence of a nonlinear atom-photon interaction [69]. Based on the SCS variational method, in the present paper we study multistability for the BEC in the optomechanical cavity. The oscillator-induced collapse

*jqliang@sxu.edu.cn
†ymyu@iphy.ac.cn
‡wliu@iphy.ac.cn

of the superradiant phase is a central effect of the system considered. As a consequence, multiple QPTs appear in the experimentally accessible parameter region. In particular, the superradiant phase can be suppressed completely at a certain high value of photon-phonon coupling and we find the direct population transfer between the two atomic levels. Moreover, the coupling-induced collapse and revival of the superradiant states are also an observation different from the BEC in an optical cavity [69] in the absence of mechanical oscillator. Finally, it may be worthwhile to remark that the SCS method is actually valid for an arbitrary atomic number N unlike the usual variation method with the Holstein-Primakoff transformation, which requires a large-N limit.

II. HAMILTONIAN AND VARIATIONAL-METHOD SOLUTIONS

Following the experiment in [23], we consider a four-level atomic ensemble in a high-finesse optical cavity of frequency ω_f with a transverse pumping [70,71] of frequency ω_p as depicted in Fig. 1. A high-quality mechanical oscillator is coupled to the cavity mode via radiation pressure [28–33]. The ultracold atoms coherently scatter pump light into the cavity mode with a position-dependent phase. An effective two-level system is obtained by eliminating adiabatically two excited states of atoms with a large frequency detuning of the pump laser [27,72]. In the optical cavity all ultracold atoms are assumed to couple identically to the single-mode field and we have an extended Dicke model, which is coupled to the mechanical oscillator. The corresponding Hamiltonian is expressed as

$$H = \omega a^\dagger a + \omega_0 S_z + \frac{U}{N} S_z a^\dagger a + \frac{g}{2\sqrt{N}}(a^\dagger + a)(S_+ + S_-) + \frac{\varsigma}{\sqrt{N}}(b^\dagger + b)a^\dagger a + \omega_b b^\dagger b, \quad (1)$$

where ω_0 is the effective two-level atom frequency, which is twice the recoil energy; $a^\dagger$ (a) is the photon creation (annihilation) operator; g denotes the collective atom-field coupling strength; $b^\dagger$ (b) is the creation (annihilation) operator of the mechanical resonator with frequency ω_b; and S_+, S_-, and S_z are the collective spin operators. The third term denotes the nonlinear atom-photon interaction resulting from the dispersive shift of the cavity frequency [23]. The effective two atomic momentum states may be denoted by $|0\rangle = |0,0\rangle$ and $|1\rangle = |\pm k, \pm k\rangle$. The atom-photon interaction takes place only for atoms of nonzero momentum state $|1\rangle$ and the interaction term is seen to be $U_0 M a^\dagger a n_1$ with $U_0 = g^2/(\omega_p - \omega_a)$, where ω_a denotes the atomic transition frequency and $M = 3/4$ is a matrix element according to the experiment [23]. In addition, n_1 and n_0 denote the collective atomic number operators in the atomic states $|1\rangle$ and $|0\rangle$, respectively. With the definition of the pseudospin operator $S_z = (n_1 - n_0)/2$ and the relation $n_1 + n_0 = N$, we obtain the nonlinear atom-photon interaction term of Eq. (1), in which the interaction constant is defined by $U = MU_0$. The effective cavity frequency is found as [69]

$$\omega = \Delta_c + U(1 + 1/M)/2 = \Delta_c + 7U/6,$$

which can be modulated by tuning the atom-photon interaction strength U and the pump-cavity field detuning $\Delta_c = \omega_f - \omega_p$. We call the detuning blue detuning for $\omega_f < \omega_p$ and red detuning for $\omega_f > \omega_p$. In addition, ς is the nonlinear photon-phonon interaction strength, which indicates the coupling between the cavity mode and mechanical oscillator via radiation pressure [28–33]. In the absence of an oscillator, the above Hamiltonian reduces to that for the BEC-cavity system [23,69].

In this paper we provide analytic solutions for the macroscopic quantum states (coherent states) in terms of the recently developed SCS variational method [69], which has the advantage that both normal $\Downarrow$ and inverted $\Uparrow$ pseudospin states can be taken into account. As a result, multiple steady states are obtained, in agreement with previous observations [24,26,27]. To this end, we begin with the partial average of the system Hamiltonian $\bar{H} = \langle\psi|H|\psi\rangle$ in the trial wave function

$$|\psi\rangle = |\alpha\rangle|\beta\rangle, \quad (2)$$

which is considered as the product of boson coherent states of the cavity mode (photon) and quantum oscillator (phonon) such that $a|\alpha\rangle = \alpha|\alpha\rangle$ and $b|\beta\rangle = \beta|\beta\rangle$ for our aim to study the macroscopic quantum states. The partial average becomes an effective Hamiltonian of the pseudospin operators only,

$$\bar{H}(\alpha,\beta) = \left(\omega + \frac{2\varsigma}{\sqrt{N}}\rho\cos\phi\right)\gamma^2 + \omega_b\rho^2 + H_{sp}(\gamma,\theta), \quad (3)$$

with the effective spin operator given by

$$H_{sp}(\gamma,\theta) = \left(\omega_0 + \frac{U}{N}\gamma^2\right)S_z + \frac{g}{\sqrt{N}}\gamma\cos\theta(S_+ + S_-),$$

where we assume that the complex eigenvalues of the boson annihilation operators have the usual form $\alpha = \gamma e^{i\theta}$ and $\beta = \rho e^{i\phi}$, respectively. The spin operator $H_{sp}(\gamma,\theta)$ as well as the total effective Hamiltonian can be directly diagonalized by means of the SCS. The four real variation parameters γ, θ, ρ, and ϕ in the trail wave function $|\psi\rangle$ are going to be determined by the variation condition. Thus we will be able to obtain the analytic stationary states and the related energies as well.

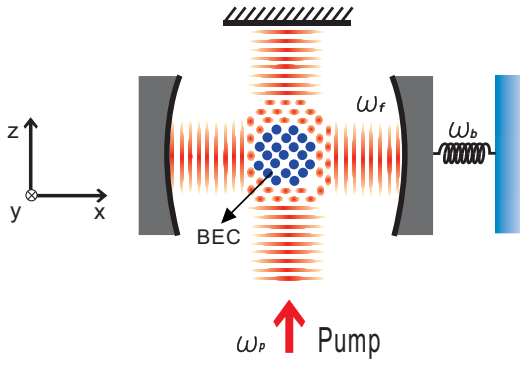

FIG. 1. Proposed experimental setup for a BEC trapped in an optomechanical cavity with a pump laser of frequency ω_p to realize the QPT. Here ω_b is the mechanical-resonator frequency and ω_f is the frequency of the cavity mode.

A. Spin-coherent-state variational method

Different from the usual variation procedure, in which the pseudospin operators are converted into a one-mode boson operator by means of the Holstein-Primakoff transformation, we start from the two eigenstates, namely, the SCSs, of the effective spin operator $H_{sp}(\gamma,\theta)$ such that

$$H_{sp}(\gamma,\theta)|\mp\mathbf{n}\rangle = E_{sp}^{\mp}(\gamma,\theta)|\mp\mathbf{n}\rangle. \tag{4}$$

The two states $|\mp\mathbf{n}\rangle$, called the SCSs of south- and north-pole gauges or normal $\Downarrow$ and inverted $\Uparrow$ spin states, are in fact the eigenstates of the spin operator $\mathbf{S}\cdot\mathbf{n}$ with the corresponding eigenvalues $\mp s$,where $s = N/2$. We assume that $\mathbf{n} = (\sin\xi\cos\eta, \sin\xi\sin\eta, \cos\xi)$ is the unit vector of the direction angles ξ and η. Thus the SCSs $|\mp\mathbf{n}\rangle$ can be generated from the maximum Dicke states $|s, \mp s\rangle$ by a rotation operator

$$R(\mathbf{n}) = e^{(\xi/2)(S_+e^{i\eta}-S_-e^{-i\eta})}$$

such that

$$|\mp\mathbf{n}\rangle = R(\mathbf{n})|s, \mp s\rangle. \tag{5}$$

We also call $|\mp\mathbf{n}\rangle$ the macroscopic quantum states, in which the minimum-uncertainty relation $\Delta S_+\Delta S_- = \langle S_z\rangle/2$ is satisfied. It is obvious that these two macroscopic quantum states are orthogonal $\langle+\mathbf{n}|-\mathbf{n}\rangle = 0$. By applying the rotation operator $R(\mathbf{n})$ to the spin operators S_z, S_+, S_- [25,73,74] we have

$$\tilde{H}_{sp}|\mp s\rangle = E_{sp}^{\mp}(\gamma,\theta)|\mp s\rangle, \tag{6}$$

where

$$\tilde{H}_{sp} = R^{\dagger}(\mathbf{n})H_{sp}(\gamma,\theta)R(\mathbf{n}) = AS_z + BS_+ + CS_-, \tag{7}$$

with

$$A(\gamma,\theta;\eta,\xi) = \left(\omega_0 + \frac{U}{N}\gamma^2\right)\cos\xi - \frac{2g}{\sqrt{N}}\gamma\cos\theta\cos\eta\sin\xi,$$

$$B(\gamma,\theta;\eta,\xi) = \left(\frac{\omega_0}{2} + \frac{U}{2N}\gamma^2\right)e^{-i\eta}\sin\xi + \frac{g}{\sqrt{N}}\gamma\cos\theta\left(\cos^2\frac{\xi}{2} - e^{-2i\eta}\sin^2\frac{\xi}{2}\right),$$

$$C(\gamma,\theta;\eta,\xi) = \left(\frac{\omega_0}{2} + \frac{U}{2N}\gamma^2\right)e^{i\eta}\sin\xi + \frac{g}{\sqrt{N}}\gamma\cos\theta\left(\cos^2\frac{\xi}{2} - e^{2i\eta}\sin^2\frac{\xi}{2}\right).$$

If the conditions

$$B(\gamma,\theta;\eta,\xi) = 0, \quad C(\gamma,\theta;\eta,\xi) = 0, \tag{8}$$

are satisfied the effective spin Hamiltonian $H_{sp}(\gamma,\theta)$ can be diagonalized in the SCSs $|\mp\mathbf{n}\rangle$ with the eigenvalues given by

$$E_{sp}^{\mp} = \mp\frac{N}{2}A(\gamma,\theta;\eta,\xi), \tag{9}$$

in which the parameters ξ and η can be determined from Eq. (8). After tedious but straightforward algebra we obtain [69]

$$A(\gamma) = \sqrt{\left(\omega_0 + \frac{U}{N}\gamma^2\right)^2 + \frac{4g^2}{N}\gamma^2}. \tag{10}$$

The average energy function in the full trail wave function

$$|\Psi_{\mp}\rangle = |\psi\rangle|\mp\mathbf{n}\rangle \tag{11}$$

is found finally as

$$E_{\mp} = \langle\Psi_{\mp}|H|\Psi_{\mp}\rangle = \left(\omega - \frac{2\varsigma}{\sqrt{N}}\rho\right)\gamma^2 + \omega_b\rho^2 + E_{sp}^{\mp}, \tag{12}$$

with the variational parameters γ and ρ to be determined from the extremum condition. The isolated phase parameter ϕ is fixed as $\cos\phi = -1$ in terms of the extremum condition with respect to ϕ for $\varsigma > 0$. The solutions of the macroscopic many-particle quantum state are found from the usual extremum conditions of the energy function

$$\frac{\partial E_{\mp}}{\partial\gamma} = \gamma\left[2\left(\omega - \frac{2\varsigma\rho}{\sqrt{N}}\right) \mp F(\gamma)\right] = 0 \tag{13}$$

with

$$F(\gamma) = \frac{N}{2}\frac{\partial A(\gamma)}{\gamma\partial\gamma} = \frac{U\left(\omega_0 + \frac{U\gamma^2}{N}\right) + 2g^2}{A(\gamma)}$$

and

$$\frac{\partial E_{\mp}}{\partial\rho} = -\frac{2\varsigma}{\sqrt{N}}\gamma^2 + 2\omega_b\rho = 0. \tag{14}$$

These conditions (13) and (14) have a trivial solution

$$\gamma = 0, \quad \rho = 0.$$

If the zero-photon-number solutions are stable with a positive second-order derivative of the energy function, namely,

$$\frac{\partial^2 E_{\mp}}{\partial\gamma^2}(\gamma_n^{\mp} = 0) > 0, \tag{15}$$

they are called the normal-phase state denoted by $N_{\mp}$ in the phase diagram. Substituting $\rho = \frac{\varsigma}{\sqrt{N}\omega_b}\gamma^2$ obtained from the extremum condition (14) into Eq. (13), the nonzero-photon-number (as well as nonzero-phonon-number) solutions are found from the equation

$$P_{\mp}(\gamma^2) = 2\left(\omega - \frac{2\varsigma^2\gamma^2}{N\omega_b}\right) \mp F(\gamma) = 0, \tag{16}$$

which, being a quartic equation of variable γ^2, can be solved graphically (see the Appendix).

The second-order derivative of the energy function [corresponding to the slope of the $P_{\mp}(\gamma^2)$ curve plotted in the Appendix] has the analytic form

$$\frac{\partial^2 E_{\mp}}{\partial\gamma^2} = 2\left(\omega - \frac{2\varsigma^2\gamma^2}{N\omega_b}\right) \mp F(\gamma) + \gamma\left[-\frac{8\varsigma^2\gamma}{N\omega_b} \mp \frac{\partial F(\gamma)}{\partial\gamma}\right], \tag{17}$$

with

$$\frac{\partial F(\gamma)}{\partial\gamma} = \frac{\gamma\left\{2U^2A^2(\gamma) - 2\left[\left(\omega_0 + \frac{U\gamma^2}{N}\right)U + 2g^2\right]^2\right\}}{NA^3(\gamma)},$$

which serves as a stability condition that $\partial^2 E_{\mp}/\partial\gamma^2 > 0$ for the stable state and is unstable otherwise. From the graphic solutions of the extremum (16) we obtain multiple stable

quantum states $S_{\mp}$ of the nonzero-photon and zero-photon states $N_{\mp}$. We will see that the multiple states result in multiple QPTs.

B. Average energy, mean photon number, and atomic population difference

From the energy function (12) we can obtain the average energy $\varepsilon_{\mp} = E_{\mp}(\gamma)/N$, which in the normal phase is

$$\varepsilon_{\mp}(\gamma_n^{\mp} = 0) = \mp\frac{\omega_0}{2}$$

and in the superradiant phase is evaluated (with the solutions $\gamma_s^{\mp}$) with

$$\varepsilon_{\mp} = \frac{E_{\mp}(\gamma_s^{\mp})}{N}. \tag{18}$$

The mean photon number is obtained as the usual average of the photon-number operator in the full trial wave function (11) with the bosonic part $|\psi\rangle = |\alpha\rangle|\beta\rangle$ defined in Eq. (2). For the stable solution $\gamma_{s\mp}$ obtained from Eq. (16) we have

$$n_p^{\mp} = \frac{\langle\Psi_{\mp}|a^{\dagger}a|\Psi_{\mp}\rangle}{N} = \bar{\gamma}_{s\mp}^2, \tag{19}$$

with $\bar{\gamma}_{s\mp}^2 = \gamma_{s\mp}^2/N$. The QPT in the Dicke model is characterized by the average photon number n_p, which serves as an order parameter, with $n_p > 0$ for the superradiant phase and $n_p = 0$ for the normal phase. The atom population difference is calculated in the state $|\Psi_{\mp}\rangle$ with the SCSs $|\mp\mathbf{n}\rangle$ given by Eq. (5),

$$\Delta n_a^{\mp} = \frac{\langle s, \mp s|R^{\dagger}(\mathbf{n})S_z R(\mathbf{n})|s, \mp s\rangle}{N} = \mp\frac{1}{2}\frac{\omega_0 + U\bar{\gamma}_{s\mp}^2}{A(\bar{\gamma}_{s\mp})}, \tag{20}$$

which reduces to the typical value in the normal phase with $\bar{\gamma}_{n\mp} = 0$ that

$$\Delta n_a^{\mp}(\bar{\gamma}_{n\mp} = 0) = \mp\tfrac{1}{2}. \tag{21}$$

III. MULTISTABILITY AND THE PHASE DIAGRAM

From the graphical solutions of the extremum (16) along with the stability condition (17) we are able to provide the phase diagram in the U-g plane for fixed photon-phonon coupling ς and pump-cavity field detuning Δ_c. In the numerical calculation we have used the experimentally realizable parameters with the atom frequency $\omega_0 = 1$ MHz. The coupling constants and energies are all measured in the unit of ω_0 throughout the paper, except the photon-phonon coupling ς. The nonlinear interaction U can vary in a wide region between ± 80 according to the experiment [23]. The reason for the use of parameter magnitudes in the actual experiment is based on the hope that the phenomena predicted in this paper can be detected experimentally by measuring the photon number. Figure 2 shows the phase diagram of blue detuning $\Delta_c = -24$ with the photon-phonon interaction strength $\varsigma = 0.2\omega_b$ [Fig. 2(a)], $\varsigma = 1.0\omega_b$ [Fig. 2(b)], $\varsigma = 2.0\omega_b$ [Fig. 2(c)], and $\varsigma = 4.0\omega_b$ [Fig. 2(d)]. The mechanical oscillator frequency is chosen as [75] $\omega_b = 2\pi \times 32.3$ MHz. As a comparison, the phase diagram of the red detuning $\Delta_c = 24$ is presented in Fig. 3 with $\varsigma = 0.2\omega_b$ [Fig. 3(a)],

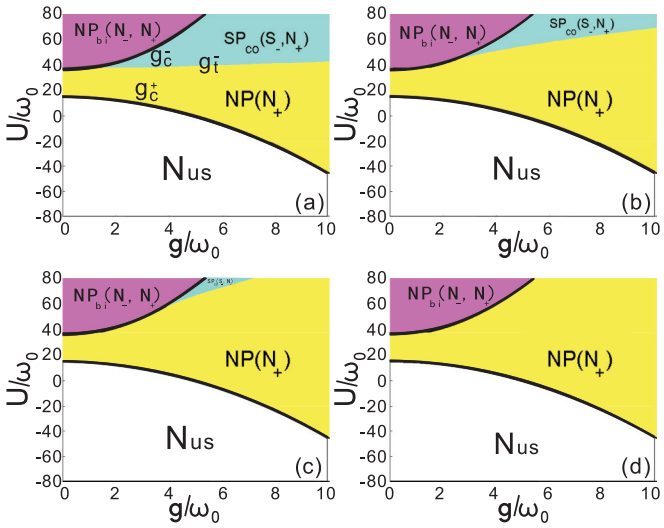

FIG. 2. Variation of the phase diagram in blue detuning $\Delta_c = -24$ with respect to the photon-phonon interaction ς. The superradiant state S_- is suppressed by the increase of ς seen in (a) $\varsigma = 0.2\omega_b$, (b) $\varsigma = 1.0\omega_b$, and (c) $\varsigma = 2.0\omega_b$ and disappears when (d) $\varsigma = 4.0\omega_b$. Here $\mathrm{NP_{bi}}(N_-,N_+)$ (pink region) denotes bistable zero-photon states of $N_{\mp}$, with N_- being the ground state and $\mathrm{SP_{co}}(S_-,N_+)$ (sea green region) means the superradiant state S_- (ground state) coexisting with the state N_+. The turning point line g_t^- induced by the oscillator is a new phase boundary between $\mathrm{SP_{co}}(S_-,N_+)$ and $\mathrm{NP}(N_+)$. Here N_{us} denotes unstable zero-photon state ($\gamma = 0$).

$\varsigma = 0.4\omega_b$ [Fig. 3(b)], $\varsigma = 0.6\omega_b$ [Fig. 3(c)], and $\varsigma = 1.0\omega_b$ [Fig. 3(d)]. From the energy extremum (16), by setting $\gamma = 0$ we can find the phase-boundary equations between normal and superradiant phases

$$g_c^{\mp} = \sqrt{\omega_0\left(\pm\omega - \frac{U}{2}\right)}, \tag{22}$$

which are independent of the photon-phonon coupling ς. The two phase-boundary lines $g_c^- = \sqrt{-24 + 2U/3}$ and $g_c^+ = \sqrt{24 - 5U/3}$ are displayed in Fig. 2 for two spin states with the blue detuning $\Delta_c = -24$. It is easy to check from the stability condition (15) that the state N_+ is located in the whole region above the phase boundary g_c^+ and N_- is restricted to the left-hand area of the boundary line g_c^-, where we have the bistable normal phase denoted by the phase notation $\mathrm{NP_{bi}}(N_-,N_+)$, with N_- being the ground state (pink region). The superradiant phase of state S_- coexisting with the inverted spin state N_+ denoted by the phase notation $\mathrm{SP_{co}}(S_-,N_+)$ is found in the area between the phase boundary g_c^- and turning point line g_t^- [sea green region in Figs. 2(a)–2(c)]. This area is identified as the superradiant phase since the superradiant state S_- has a lower energy (ground state). The region of superradiant state S_- is suppressed with the increase of photon-phonon coupling ς by the damping of the mechanical oscillator [Figs. 2(a)–2(c)] and quenched completely when $\varsigma = 4.0\omega_b$ as shown in Fig. 2(d). The turning point line is therefore a phase boundary between the superradiant phase and the normal phase of state N_+ with the phase notation $\mathrm{NP}(N_+)$ (yellow region). Thus we have two QPTs at the critical point g_c^- and

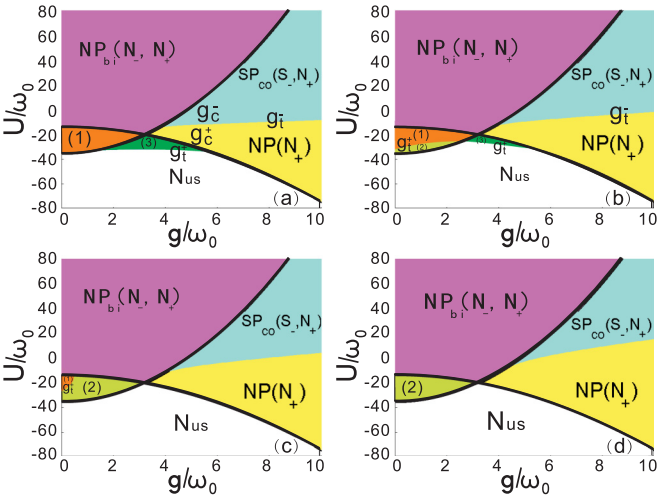

FIG. 3. Phase diagram of red detuning $\Delta_c = 24$. The two phase boundary lines $g_c^{\mp}$ cross at the point $g_c^- = g_c^+$, forming an overlap region in which $\mathrm{NP_{co}}(N_-,S_+)$ [orange region, labeled (1)] is located. The state S_+ extends to the region below the two boundary lines $g_c^{\mp}$ [green region, labeled (3)] and becomes a ground state $\mathrm{SP}(S_+)$. The total area of state S_+ with the lower boundary line g_t^+ is suppressed continuously with the increase of (a) $\varsigma = 0.2\omega_b$, (b) $0.4\omega_b$, (c) $0.6\omega_b$, and (d) $1.0\omega_b$. Correspondingly, the area of $\mathrm{NP}(N_-)$ [apple green region, labeled (2)] increases.

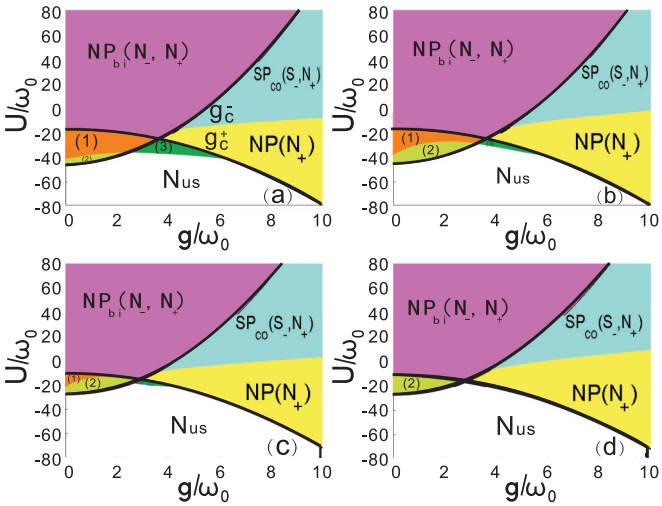

FIG. 4. Variation of the phase diagram with respect to red detuning (a) and (b) $\Delta_c = 30$ and (c) and (d) $\Delta_c = 18$ and photon-phonon interaction (a) and (c) $\varsigma = 0.4\omega_b$ and (b) and (d) $\varsigma = 0.6\omega_b$. The area of state S_+ in $\mathrm{NP_{co}}(N_-,S_+)$ and $\mathrm{SP}(S_+)$ increases with the detuning Δ_c and decreases with the photon-phonon coupling ς. (d) The state S_+ even disappears completely when $\Delta_c = 18$ at a lower value of photon-phonon coupling $\varsigma = 0.6\omega_b$.

turning point g_t^-, respectively. In addition, the photon-phonon coupling results in a dynamically unstable macroscopic state S_{us}^- not appearing in the phase diagram. For the red detuning $\Delta_c = 24$ the two phase-boundary lines $g_c^- = \sqrt{24 + 2U/3}$ and $g_c^+ = \sqrt{-24 - 5U/3}$ shown in Fig. 3 cross at the point $g_c^- = g_c^+$ $(U = -144/7)$, forming an overlap region with richer structure. In the overlap area, the normal-phase notation $\mathrm{NP_{co}}(N_-,S_+)$ [orange region, labeled (1)] means the ground state N_- of zero photon coexisting with the superradiant state S_+. This region decreases with the increase of photon-phonon coupling ς due to the mechanical-oscillator-induced collapse of the superradiant state S_+ [Figs. 3(a)–3(c)]. The area left over [apple green, labeled (2)] becomes a simple normal phase $\mathrm{NP}(N_-)$ [Figs. 3(b) and 3(c)], which finally occupies the whole overlap region because of the complete quenching of state S_+ when $\varsigma = 1.0\omega_b$ [Fig. 3(d)]. The state S_+ extending away from the overlap area becomes a simple superradiant phase $\mathrm{SP}(S_+)$ as shown in Figs. 3(a)and 3(b) [green region, labeled (3)]. Here N_{us} denotes unstable zero-phonon states, which are solutions of both extremum equations $P_{\mp}(\gamma^2 = 0) = 0$ with the negative second-order derivative $\partial^2 E_{\mp}/\partial\gamma^2(\gamma = 0) < 0$. We will see that the convex phase-boundary line g_t^+, particularly in Fig. 3(b), is responsible for the collapse and revival of the superradiant state S_+.

To see the area variation of state S_+ with respect to Δ_c and ς, we present the phase diagrams in Fig. 4 for red detuning $\Delta_c = 30$ [Figs. 4(a) and 4(b)] and $\Delta_c = 18$ [Figs. 4(c) and 4(d)] with $\varsigma = 0.4\omega_b$ [Figs. 4(a) and 4(c)] and $\varsigma = 0.6\omega_b$ [Figs. 4(b) and 4(d)]. It can be seen that the area of state S_+ in $\mathrm{NP_{co}}(N_-,S_+)$ and $\mathrm{SP}(S_+)$ increases with the detuning Δ_c and decreases with the photon-phonon coupling ς by comparing Figs. 4(a)and 4(c) and Figs. 4(b) and 4(d) with Figs. 4(a) and 4(b) and Figs. 4(c) and 4(d). The state S_+ even disappears completely when $\Delta_c = 18$ at a lower value of photon-phonon coupling $\varsigma = 0.6\omega_b$ [Fig. 4(d)].

The additional phase boundary $g_t^{\mp}$ induced by the collapse of superradiant states $S_{\mp}$ is an observation that, different from the BEC-cavity system [69], results in multiple QPTs in the experimentally accessible coupling-constant region $g \in [0,10]$.

IV. MULTIPLE QUANTUM PHASE TRANSITIONS AND THE ATOMIC POPULATION TRANSFER

To show clearly the multistability and multiple QPTs we present in Fig. 5 the variation curves of the average photon number n_p [Figs. 5(a1)–5(c1)], the atomic population difference Δn_a [Figs. 5(a2)–5(c2)], and the average energy ε [Figs. 5(a3)–5(c3)] with respect to the coupling constant g for blue detuning $\Delta_c = -24$ and the positive atom-photon interaction $U = 65$. The curves are plotted in different photon-phonon interaction values $\varsigma = 1.0\omega_b$ [Figs. 5(a1)–5(a3)], $\varsigma = 2.0\omega_b$ [Figs. 5(b1)–5(b3)], $\varsigma = 4.0\omega_b$ [Figs. 5(c1)–5(c3)] in order to demonstrate the effect of oscillator on the QPT.

For the lower value of ς [Figs. 5(a1)–5(a3)], we have bistable normal-phase states N_- (black solid line) and N_+ (red dashed line) below the critical value g_c^- (pink region in Fig. 2). Here N_- is the ground state with lowest energy [Fig. 5(a3)] and atomic population as well [Fig. 5(a2)]. In addition, there exists an unstable state S_{us}^- (blue dotted line) in this region corresponding to the unstable solution γ_{us}^- in Fig. 7. The QPT from $\mathrm{NP_{bi}}(N_-,N_+)$ to $\mathrm{SP_{co}}(S_-,N_+)$ takes place at the critical point $g_c^- = 4.3970$ evaluated from the boundary line (22). The superradiant state S_- (black solid line), i.e., the stable solution γ_s^- in Fig. 7, and zero-photon state N_+ along with the unstable state S_{us}^- are located in the region (sea

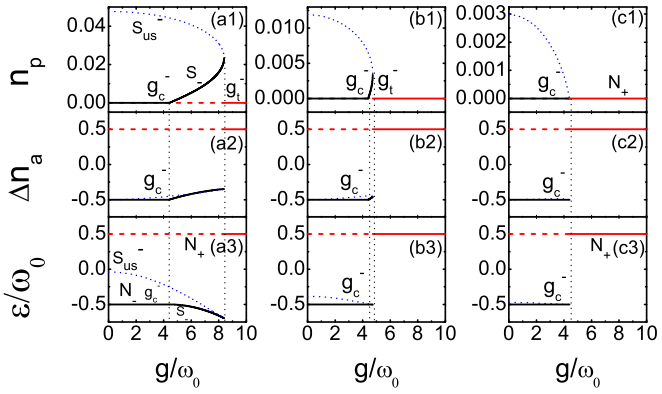

FIG. 5. Mean photon number n_p, atom population difference Δn_a, and average energy ε vs atom-field coupling strength g in the blue detuning $\Delta_c = -24$ and positive atom-photon interaction $U = 65$. The effect of photon-phonon interaction on the multiple QPTs is displayed in (a) $\varsigma = 1.0\omega_b$, (b) $\varsigma = 2.0\omega_b$, and (c) $\varsigma = 4.0\omega_b$. The increase of ς from (a) to (c) does not affect the critical point g_c^- of the usual QPT [in fact, NP(N_-) $\rightarrow$ SP(S_-)]. (c) However, the transition point g_t^- of the inverted QPT SP(S_-) $\rightarrow$ NP(N_+) shifts back and finally coincides with g_c^-, resulting in the atomic population transfer between two states N_- and N_+. With the decrease of ζ the region of SP(S_-) increases and extends to infinity when $\zeta = 0$. Thus the QPT reduces to that of the normal Dicke model. Here S_{us}^- denotes the dynamically unstable state of normal spin $\Downarrow$ corresponding to the unstable nonzero-photon-number solution γ_{us}^- shown in Fig. 7.

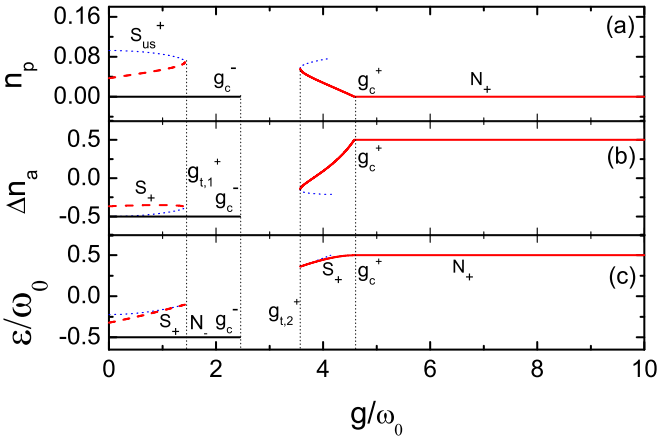

FIG. 6. The n_p, Δn_a, and ε curves in red detuning $\Delta_c = 24$ with negative atom-photon interaction $U = -27$ and $\varsigma = 0.4\omega_b$. The superradiant state S_+ collapses at the turning point $g_{t,1}^+$ and revives at $g_{t,2}^+$. Here g_c^+ is the critical point of the inverted QPT from SP(S_+) to NP(N_+). There is no stable state in the region (blank area in the phase diagram) between g_c^- and $g_{t,2}^+$, but there is an unstable zero-photon state N_{us}. Here S_{us}^+ denotes the unstable state of inverted spin $\Uparrow$ corresponding to the unstable nonzero-photon-number solution γ_{us}^+ shown in Fig. 9.

green in the phase diagram in Fig. 2) between critical point g_c^- and turning point $g_t^- \approx 8.4$ [see also Fig. 7(c)], where the superradiant state S_- collapses and the photon-number curve n_p of state S_- turns back, joining with the blue dotted line of state S_{us}^- [Fig. 5(a1)]. The system undergoes the second QPT from SP$_{co}$(S_-, N_+) to NP(N_+) at g_t^-. The inverted spin state N_+ becomes the ground state in this region due to the collapse of S_-. The position of the turning point g_t^- shifts toward the lower value direction of g with the increase of the photon-phonon interaction ς [see Figs. 5(a) and 5(b)] and coincides with the critical point g_c^- at $\varsigma = 4.0\omega_b$ [Fig. 5(c)]. In this case the superradiant phase disappears completely by resonant damping of the mechanical oscillator, resulting in the coupling-induced population transfer from N_- ($\Downarrow$) to N_+ ($\Uparrow$) (i.e., the spin flip) in the vacuum ($n_p = 0$). Since the atomic population inversion plays an important role in laser physics, the manipulation of population transfer may have technical applications.

V. COLLAPSE AND REVIVAL OF THE SUPERRADIANT STATE AND INVERTED QUANTUM PHASE TRANSITION

To reveal the phenomena in the red detuning and negative atom-photon coupling we plot the curves of n_p, Δn_a, and ε in Figs. 6(a)–6(c), respectively, for $\Delta_c = 24$ and $U = -27$ corresponding to the graphical solutions of Fig. 9. Below the turning point $g_{t,1}^+ \approx 1.42$, we have NP$_{co}$(N_-, S_+) [orange region in the phase diagram of Fig. 3(b)]. The ground state N_- (black solid line) coexists with the superradiant state S_+ (red dashed line) and the unstable state S_{us}^+ (blue dotted line). The superradiant state S_+ collapses at the turning point $g_{t,1}^+$ and the single normal-phase state N_- remains alone, denoted by NP(N_-) (apple green in the overlap region of phase diagram). Here NP(N_-) extends continuously to the critical point $g_c^- = 2.4495$. Since the turning point line g_t^+ is a convex curve in the phase diagram in Fig. 3(b), the horizontal line of $U = -27$ crosses the curved line at two points $g_{t,1}^+$ within the overlap region and $g_{t,2}^+$ outside it. Between the critical point g_c^- and turning point $g_{t,2}^+ \approx 3.6$ there is no stable state but there is an unstable zero-photon state N_{us}, which can also be seen from the phase diagram in Fig. 3 (blank region). Beyond the turning point $g_{t,2}^+$ the superradiant state S_+ is revived and becomes a ground state (red solid line) identified by the phase notation SP(S_+). We also see a short branch of the unstable state S_{us}^+ (blue dotted line), which, however, turns to the right, which is different from the behavior at the turning point $g_{t,1}^+$. An inverted QPT from SP(S_+) to NP(N_+) is observed at the critical point $g_c^+ = 4.5826$. This transition is in the opposite direction compared with the usual QPT in the Dicke model. The inverted transition may be due to the negative effective frequency ($\omega < 0$) in the red detuning case [69].

VI. CONCLUSION AND DISCUSSION

The SCS variational method provides a possibility to study multiple stable macroscopic quantum states generated by the variation of the atom-photon interaction U and pump-cavity field detuning Δ_c. The SP(S_+) and NP(N_+) resulting from the inverted pseudospin exist in the red detuning region with the negative atom-photon interaction ($U < 0$). The inverted QPT from SP(S_+) to NP(N_+) is observed with an increase of the atom-field coupling constant g. The mechanical oscillator does not have any effect in the field vacuum, but can greatly

affect the superradiant phase since it is coupled to the cavity mode through the radiation pressure. In particular, the radiation field in the states $S_{\mp}$ can be damped to zero when the atom-field coupling g increases to a certain value called the turning points $g_t^{\mp}$, which depend also on the photon-phonon coupling strength ς. This behavior is quite different from the Dicke model, in which the photon number increases with the coupling g. The collapse of superradiant states S_- leads to the second QPT actually from SP(S_-) to NP(N_+) at the turning point g_t^-. The multiple QPTs are the key observation, which, not existing in the BEC-cavity system [69], has conceptual importance in the cavity optomechanics. The superradiant state S_- disappears at higher value of the photon-phonon coupling, for example, $\varsigma = 4.0\omega_b$ in the case considered in Fig. 5(c). We find the direct population transfer from N_- to N_+ in the vacuum, i.e., the spin flip from the normal $\Downarrow$ to the inverted $\Uparrow$ pseudospin states [26,69]. Since the atom population inversion plays a important role in laser physics, the manipulation of atomic population transfer (or spin flip) may have technical applications.

The mechanical oscillator also induces the dual (nonzero photon) solutions $\gamma_s^{\mp}$ and $\gamma_{\rm us}^{\mp}$ of the energy extremum (16), which is a quartic equation of variable γ^2 instead of the quadratic equation in the BEC-cavity system [69]. However, the upper-branch solutions $\gamma_{\rm us}^{\mp}$ are unstable with a negative second-order derivative of the energy function. In the red detuning and negative U regions we observe an interesting phenomenon of the collapse and revival of state S_+ followed by the inverted QPT of SP(S_+) $\rightarrow$ NP(N_+). The coupling-induced collapse and revival may be a typical phenomenon of the nonlinear photon-phonon interaction, since the phase boundary line g_t^+ is a convex curve, which has two cross points with the horizontal line of $U = -27$ in the phase diagram in Fig. 3(b).

The QPT demonstrated by the SCS variational method is valid for arbitrary atomic number N. In the absence of both an atom-photon interaction ($U = 0$) and a photon-phonon interaction ($\varsigma = 0$) the QPT obtained in the present paper is exactly that [17,76] in the Dicke model, however, the thermodynamic limit ($N \rightarrow \infty$) is not studied. In particular, the QPT remains the same for the Rabi model with $N = 1$, in agreement with recent observation [77].

ACKNOWLEDGMENTS

This work was partially supported by the National Natural Science Foundation of China under Grants No. 11275118, No. 11434015, No. 61227902, No. 61378017, No. 61275129, and No. 11404216; NKBRSFC under Grants No. 2011CB921502 and No. 2012CB821305; SKLQOQOD under Grant No. KF201403; SPRPCAS under Grant No. XDB01020300; and the Starting Research Funds from the Shaoxing University under Grant No. 20145025 (J.L.).

APPENDIX: GRAPHICAL SOLUTIONS OF THE EXTREMUM EQUATION

For blue detuning and positive U only the normal spin $\Downarrow$ is possible to fulfill the extremum (16). The two nonzero-photon-number solutions γ_s^- and $\gamma_{\rm us}^-$ are zero points of the polynomial curve $P_-(\gamma^2)$ as shown in Fig. 7(b1). The lower value solution γ_s^- is stable with a positive curve slope (i.e., positive second-order derivative) and therefore is called the superradiant state, denoted by S_-. It corresponds to the local energy minimum as shown in Fig. 7(b2), while the higher value solution $\gamma_{\rm us}^-$ is unstable with a negative curve slope [Fig. 7(b1)]. We call the unstable nonzero-photon-number solution the dynamically unstable macroscopic state, denoted by $S_{\rm us}^-$, which is a local energy maximum [Fig. 7(b2)]. The two

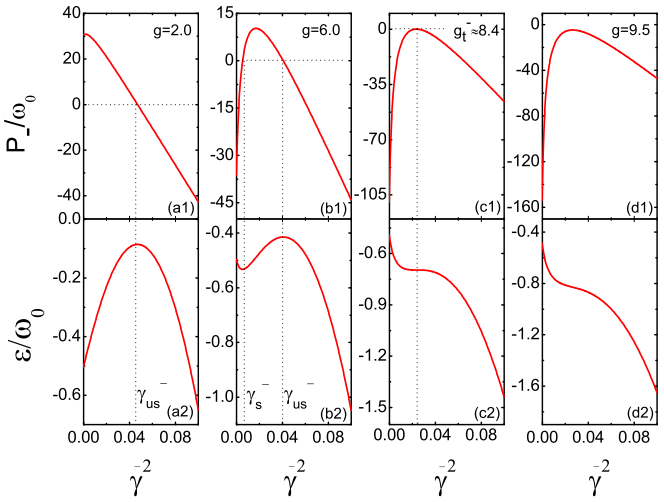

FIG. 7. (a1)–(d1) Graphical solutions of the extremum equation $P_-(\gamma^2) = 0$ and (a2)–(d2) the corresponding average energy ε vs the mean photon number $\bar{\gamma}^2 = \gamma^2/N$ with $\Delta_c = -24$, $\varsigma = 1.0\omega_b$, and $U = 65$. The atom-field coupling dependence of the solution is shown in (a) $g = 2.0$, (b) $g = 6.0$, (c) $g_t^- \approx 8.4$ (turning point), and (d) $g = 9.5$. Here γ_s^- and $\gamma_{\rm us}^-$ denote the stable and unstable nonzero-photon solutions.

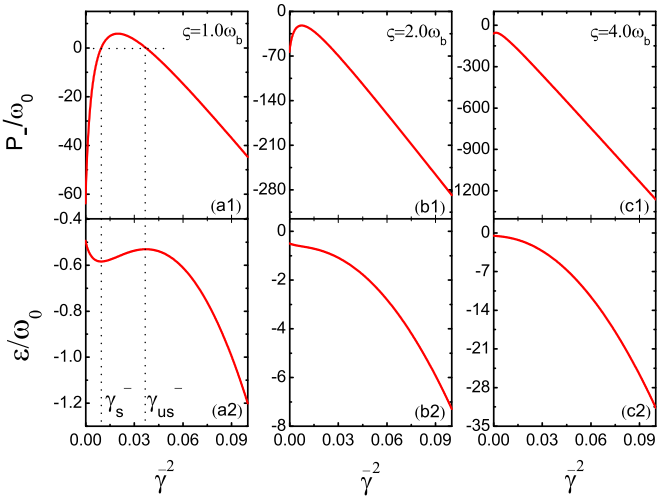

FIG. 8. Photon-phonon interaction dependence of the graphical solutions and the related energy with $\Delta_c = -24$, $g = 7.0$, and $U = 65$ for (a) $\varsigma = 1.0\omega_b$, (b) $\varsigma = 2.0\omega_b$, and (c) $\varsigma = 4.0\omega_b$. The extremum equation $P_-(\gamma^2) = 0$ does not have a nonzero-photon solution at the higher values of ς shown in (b) and (c) due to the resonant damping of the mechanical oscillator.

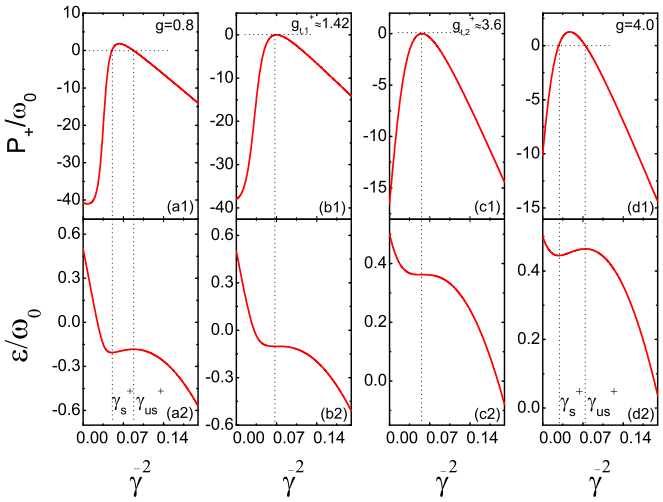

FIG. 9. Graphical solutions of $P_+(\gamma^2)=0$ with red detuning $\Delta_c=24$, $\varsigma=0.4\omega_b$, and $U=-27$. The g dependence is displayed in (a) $g=0.8$, (b) $g^+_{t,1}\approx 1.42$ (turning point), (c) $g^+_{t,2}\approx 3.6$ (turning point), and (d) $g=4.0$. The solution γ_s^+ (superradiant state S_+ in the phase diagram) collapses at $g^+_{t,1}$ and revives at $g^+_{t,2}$.

solutions are close to each other when the field-atom coupling increases and finally coincide at $g_t^-\approx 8.4$, where the energy function becomes a flex point in Fig. 7(c2), which we call the turning point. Beyond the turning point the extremum (16) no longer has a nonzero-photon solution [Fig. 7(d)]. The unstable solution $\gamma_{\rm us}^-$ extends to the lower-coupling-value region $g=2.0$ below the critical point g_c^-, as shown in Fig. 7(a), where the stable solution γ_s^- does not exist (see Fig. 5 for the critical point g_c^-). Figure 8 shows the effect of photon-phonon coupling ς that the two solutions move toward the lower value of γ with an increase of ς for the given $g=7.0$. The stable nonzero-photon-number solution γ_s^- no longer exists when $\varsigma=4.0\omega_b$ [Fig. 8(c)]. The situation becomes very different for the red detuning and negative U region, where the inverted spin $\Uparrow$ is the solution. For the lower atom-field coupling value $g=0.8$ the nonzero-photon stable solution γ_s^+ of the equation $P_+(\gamma^2)=0$ in Fig. 9(a) is an excited state denoted by S_+. Between the two turning points $g^+_{t,1}\approx 1.42$ and $g^+_{t,2}\approx 3.6$ [Figs. 9(b) and 9(c)] the nonzero solution γ_s^+ collapses. It is revived, however, beyond the turning point $g^+_{t,2}\approx 3.6$ accompanying an unstable solution $\gamma_{\rm us}^+$ [Fig. 9(d)], which we denote by $S_{\rm us}^+$ in the phase diagram.

[1] M. H. Anderson, J. R. Ensher, M. R. Matthews, C. E. Wieman, and E. A. Cornell, Science **269**, 198 (1995).
[2] K. B. Davis, M.-O. Mewes, M. R. Andrews, N. J. van Druten, D. S. Durfee, D. M. Kurn, and W. Ketterle, Phys. Rev. Lett. **75**, 3969 (1995).
[3] I. Bloch, J. Dalibard, and S. Nascimbene, Nat. Phys. **8**, 267 (2012).
[4] I. Bloch, J. Dalibard, and W. Zwerger, Rev. Mod. Phys. **80**, 885 (2008).
[5] L. Zhou, H. Pu, K. Zhang, X. D. Zhao, and W. Zhang, Phys. Rev. A **84**, 043606 (2011).
[6] V. M. Stojanovic, C. Wu, W. V. Liu, and S. DasSarma, Phys. Rev. Lett. **101**, 125301 (2008).
[7] V. S. Shchesnovich and V. V. Konotop, Phys. Rev. Lett. **102**, 055702 (2009).
[8] Y. V. Bludov and V. V. Konotop, Phys. Rev. A **81**, 013625 (2010).
[9] H. Hu, B. Ramachandhran, H. Pu, and X. J. Liu, Phys. Rev. Lett. **108**, 010402 (2012).
[10] X.-F. Zhou, J. Zhou, and C. J. Wu, Phys. Rev. A **84**, 063624 (2011).
[11] H. Ritsch, P. Domokos, F. Brennecke, and T. Esslinger, Rev. Mod. Phys. **85**, 553 (2013).
[12] B. Padhi and S. Ghosh, Phys. Rev. Lett. **111**, 043603 (2013).
[13] Y. Colombe, T. Steinmetz, G. Dubois, F. Linke, D. Hunger, and J. Reichel, Nature (London) **450**, 272 (2007).
[14] O. Castaños, E. Nahmad-Achar, R. López-Peña, and J. G. Hirsch, Phys. Rev. A **86**, 023814 (2012).
[15] R. H. Dicke, Phys. Rev. **93**, 99 (1954).
[16] P. Zanardi, M. G. A. Paris, and L. Campos Venuti, Phys. Rev. A **78**, 042105 (2008).
[17] C. Emary and T. Brandes, Phys. Rev. E **67**, 066203 (2003).
[18] F. Brennecke, T. Donner, S. Ritter, T. Bourdel, M. Köhl, and T. Esslinger, Nature (London) **450**, 268 (2007).
[19] A.-C. Ji, X. C. Xie, and W. M. Liu, Phys. Rev. Lett. **99**, 183602 (2007).
[20] A.-C. Ji, Q. Sun, X. C. Xie, and W. M. Liu, Phys. Rev. Lett. **102**, 023602 (2009).
[21] X.-F. Zhang, Q. Sun, Y.-C. Wen, W. M. Liu, S. Eggert, and A.-C. Ji, Phys. Rev. Lett. **110**, 090402 (2013).
[22] K. Baumann, R. Mottl, F. Brennecke, and T. Esslinger, Phys. Rev. Lett. **107**, 140402 (2011).
[23] K. Baumann, C. Guerlin, F. Brennecke, and T. Esslinger, Nature (London) **464**, 1301 (2010).
[24] V. M. Bastidas, C. Emary, B. Regler, and T. Brandes, Phys. Rev. Lett. **108**, 043003 (2012).
[25] Z.-D. Chen, J.-Q. Liang, S.-Q. Shen, and W.-F. Xie, Phys. Rev. A **69**, 023611 (2004).
[26] M. J. Bhaseen, J. Mayoh, B. D. Simons, and J. Keeling, Phys. Rev. A **85**, 013817 (2012).
[27] N. Liu, J. D. Li, and J.-Q. Liang, Phys. Rev. A **87**, 053623 (2013).
[28] T. J. Kippenberg and K. J. Vahala, Science **321**, 1172 (2008).
[29] F. Marquardt and S. M. Girvin, Physics **2**, 40 (2009).
[30] I. Favero and K. Karrai, Nat. Photon. **3**, 201 (2009).
[31] M. Aspelmeyer, S. Gröblacher, K. Hammerer, and N. Kiesel, J. Opt. Soc. Am. B **27**, A189 (2010).
[32] C. A. Regal and K. W. Lehnert, J. Phys.: Conf. Ser. **264**, 012025 (2011).
[33] S. G. Hofer, W. Wieczorek, M. Aspelmeyer, and K. Hammerer, Phys. Rev. A **84**, 052327 (2011).
[34] F. Marquardt, J. P. Chen, A. A. Clerk, and S. M. Girvin, Phys. Rev. Lett. **99**, 093902 (2007).
[35] Y. Li, L. A. Wu, and Z. D. Wang, Phys. Rev. A **83**, 043804 (2011).
[36] O. Arcizet, P.-F. Cohadon, T. Briant, M. Pinard, and A. Heidmann, Nature (London) **444**, 71 (2006).
[37] Y.-S. Park and H. Wang, Nat. Phys. **5**, 489 (2009).

[38] I. Wilson-Rae, N. Nooshi, W. Zwerger, and T. J. Kippenberg, Phys. Rev. Lett. **99**, 093901 (2007).
[39] C. Genes, D. Vitali, P. Tombesi, S. Gigan, and M. Aspelmeyer, Phys. Rev. A **77**, 033804 (2008).
[40] J.-Q. Liao, H. K. Cheung, and C. K. Law, Phys. Rev. A **85**, 025803 (2012).
[41] S. Mancini and P. Tombesi, Phys. Rev. A **49**, 4055 (1994).
[42] S. Bose, K. Jacobs, and P. L. Knight, Phys. Rev. A **56**, 4175 (1997).
[43] A. Mari and J. Eisert, Phys. Rev. Lett. **103**, 213603 (2009).
[44] J. Q. Liao and C. K. Law, Phys. Rev. A **83**, 033820 (2011).
[45] S. Mancini, V. Giovannetti, D. Vitali, and P. Tombesi, Phys. Rev. Lett. **88**, 120401 (2002).
[46] M. Paternostro, D. Vitali, S. Gigan, M. S. Kim, C. Brukner, J. Eisert, and M. Aspelmeyer, Phys. Rev. Lett. **99**, 250401 (2007).
[47] A. Ferreira, A. Guerreiro, and V. Vedral, Phys. Rev. Lett. **96**, 060407 (2006).
[48] S. Gröblacher, K. Hammerer, M. R. Vanner, and M. Aspelmeyer, Nature (London) **460**, 724 (2009).
[49] M. J. Hartmann and M. B. Plenio, Phys. Rev. Lett. **101**, 200503 (2008).
[50] C. Fabre, M. Pinard, S. Bourzeix, A. Heidmann, E. Giacobino, and S. Reynaud, Phys. Rev. A **49**, 1337 (1994).
[51] T. J. Kippenberg, H. Rokhsari, T. Carmon, A. Scherer, and K. J. Vahala, Phys. Rev. Lett. **95**, 033901 (2005).
[52] S. Gigan, H. R. Böhm, M. Paternostro, F. Blaser, G. Langer, J. B. Hertzberg, K. C. Schwab, D. Bäuerle, M. Aspelmeyer, and A. Zeilinger, Nature (London) **444**, 67 (2006).
[53] V. B. Braginsky and A. B. Manukin, Sov. Phys. JETP **52**, 986 (1967).
[54] O. Arcizet, P. F. Cohadon, T. Briant, M. Pinard, A. Heidmann, J. M. Mackowski, C. Michel, L. Pinard, O. Francais, and L. Rousseau, Phys. Rev. Lett. **97**, 133601 (2006).
[55] A. Dorsel, J. D. McCullen, P. Meystre, E. Vignes, and H. Walther, Phys. Rev. Lett. **51**, 1550 (1983).
[56] T. Corbitt, D. Ottaway, E. Innerhofer, J. Pelc, and N. Mavalvala, Phys. Rev. A **74**, 021802(R) (2006).
[57] B. S. Sheard, M. B. Gray, C. M. Mow-Lowry, D. E. McClelland, and S. E. Whitcomb, Phys. Rev. A **69**, 051801(R) (2004).
[58] T. Corbitt, Y. Chen, E. Innerhofer, H. Muller-Ebhardt, D. Ottaway, H. Rehbein, D. Sigg, S. Whitcomb, C. Wipf, and N. Mavalvala, Phys. Rev. Lett. **98**, 150802 (2007).
[59] S. Gupta, K. L. Moore, K. W. Murch, and D. M. Stamper-Kurn, Phys. Rev. Lett. **99**, 213601 (2007).
[60] E. Verhagen, S. Deléglise, S. Weis, A. Schliesser, and T. J. Kippenberg, Nature (London) **482**, 63 (2012).
[61] J. P. Santos, K. Furuya, and F. L. Semião, Phys. Rev. A **82**, 063801 (2010).
[62] Y. Dong, J. Ye, and H. Pu, Phys. Rev. A **83**, 031608(R) (2011).
[63] A. A. Clerk, F. Marquardt, and J. G. E. Harris, Phys. Rev. Lett. **104**, 213603 (2010).
[64] T. P. Purdy, D. W. C. Brooks, T. Botter, N. Brahms, Z.-Y. Ma, and D. M. Stamper-Kurn, Phys. Rev. Lett. **105**, 133602 (2010).
[65] J. D. Thompson, B. M. Zwickl, A. M. Jayich, Florian Marquardt, S. M. Girvin, and J. G. E. Harris, Nature (London) **452**, 72 (2008).
[66] J. C. Sankey, C. Yang, B. M. Zwickl, A. M. Jayich, and J. G. E. Harris, Nat. Phys. **6**, 707 (2010).
[67] J. Lian, N. Liu, J.-Q. Liang, G. Chen, and S. T. Jia, Phys. Rev. A **88**, 043820 (2013).
[68] J. Keeling, M. J. Bhaseen, and B. D. Simons, Phys. Rev. Lett. **105**, 043001 (2010).
[69] X. Q. Zhao, N. Liu, and J.-Q. Liang, Phys. Rev. A **90**, 023622 (2014).
[70] G. Szirmai, D. Nagy, and P. Domokos, Phys. Rev. A **81**, 043639 (2010).
[71] N. Liu, J. Lian, J. Ma, L. T. Xiao, G. Chen, J.-Q. Liang, and S. T. Jia, Phys. Rev. A **83**, 033601 (2011).
[72] D. Nagy, G. Kónya, G. Szirmai, and P. Domokos, Phys. Rev. Lett. **104**, 130401 (2010).
[73] Y.-Z. Lai, J.-Q. Liang, H. J. W. Müller-Kirsten, and J. G. Zhou, J. Phys. A: Math. Gen. **29**, 1773 (1996).
[74] Y.-Z. Lai, J.-Q. Liang, H. J. W. Müller-Kirsten, and J. G. Zhou, Phys. Rev. A **53**, 3691 (1996).
[75] F. Massel, S. U. Cho, J. Pirkkalainen, P. J. Hakonen, T. T. Heikkilä, and M. A. Sillanpää, Nat. Commun. **3**, 987 (2012).
[76] G. Chen, J. Q. Li, and J.-Q. Liang, Phys. Rev. A **74**, 054101 (2006).
[77] M.-J. Hwang, R. Puebla, and M. B. Plenio, Phys. Rev. Lett. **115**, 180404 (2015).